A high-resolution record of surface melt on Antarctic ice shelves using multi-source remote sensing data and deep learning

de Roda Husman, Sophie; Lhermitte, Stef; Bolibar, Jordi; Izeboud, Maaike; Hu, Zhongyang; Shukla, Shashwat; van der Meer, Marijn; Long, David; Wouters, Bert

DOI
10.1016/j.rse.2023.113950

Publication date
2023

Document Version
Final published version

Published in
Remote Sensing of Environment

Citation (APA)
de Roda Husman, S., Lhermitte, S., Bolibar, J., Izeboud, M., Hu, Z., Shukla, S., van der Meer, M., Long, D., & Wouters, B. (2023). A high-resolution record of surface melt on Antarctic ice shelves using multi-source remote sensing data and deep learning. *Remote Sensing of Environment*, *301*, Article 113950. https://doi.org/10.1016/j.rse.2023.113950

Remote Sensing of Environment 301 (2024) 113950

Contents lists available at ScienceDirect

Remote Sensing of Environment

journal homepage: www.elsevier.com/locate/rse

A high-resolution record of surface melt on Antarctic ice shelves using multi-source remote sensing data and deep learning

Sophie de Roda Husman [a,*], Stef Lhermitte [c,a], Jordi Bolibar [a], Maaike Izeboud [a], Zhongyang Hu [b], Shashwat Shukla [a], Marijn van der Meer [d], David Long [e], Bert Wouters [a]

[a] Department of Geoscience & Remote Sensing, Delft University of Technology, Delft, The Netherlands
[b] Institute for Marine and Atmospheric Research Utrecht, Utrecht University, Utrecht, The Netherlands
[c] Department of Earth & Environmental Sciences, KU Leuven, Leuven, Belgium
[d] Laboratory of Hydraulics, Hydrology and Glaciology (VAW), ETH Zürich, Zürich, Switzerland
[e] Department of Electrical and Computer Engineering, Brigham Young University, Provo, UT, USA

ARTICLE INFO

Edited by Menghua Wang

Dataset link: https://github.com/SdeRodaHusman/UMelt, https://doi.org/10.4121/8a8934ef-9407-406f-8bfb-573eb182ec54.v1, https://code.earthengine.google.com/?asset=projects/phd-detectionsurfacemelt/assets/UMelt_Antarctica/MeltSeasonXXXX/UMelt_AllData_MeltSeasonXXXX, https://doi.org/10.4121/8a8934ef-9407-406f-8bfb-573eb182ec54.v1, https://code.earthengine.google.com/?asset=projects/phd-detectionsurfacemelt/assets/UMelt_Antarctica/MeltSeasonXXXX/UMelt_MeltFraction_MeltSeasonXXXX

Keywords:
Antarctica
U-Net
Machine learning
Microwave remote sensing
Enhanced resolution
Google Earth Engine
Surface melt

ABSTRACT

While the influence of surface melt on Antarctic ice shelf stability can be large, the duration and affected area of melt events are often small. Therefore, melt events are difficult to capture with remote sensing, as satellite sensors always face the trade-off between spatial and temporal resolution. To overcome this limitation, we developed UMelt: a surface melt record for all Antarctic ice shelves with a high spatial (500 m) and high temporal (12 h) resolution for the period 2016–2021. Our approach is based on a deep learning model, specifically a U-Net, which was developed in Google Earth Engine. The U-Net combines microwave remote sensing observations from three sources: Sentinel-1, Special Sensor Microwave Imager/Sounder (SSMIS), and Advanced Scatterometer (ASCAT). The U-Net was trained on the Shackleton Ice Shelf for melt seasons 2017–2021, using the fine-scale melt patterns of Sentinel-1 as reference data and SSMIS, ASCAT, a digital elevation model, and multi-year Sentinel-1 melt fraction as predictors. The trained U-Net performed well on the Shackelton Ice Shelf for test melt season 2016–2017 (accuracy: 91.3%; F1-score: 86.9%), and the Larsen C Ice Shelf, which was not considered during training (accuracy: 91.0%; F1-score: 89.3%). Using the trained U-Net model, we have successfully developed the UMelt record. UMelt allows Antarctic-wide surface melt to be detected at a small scale while preserving a high temporal resolution, which could lead to new insights into the response of ice shelves to a changing atmospheric forcing.

1. Introduction

Antarctica's ice shelves, the floating extensions of the grounded ice sheet, are crucial in regulating sea level rise (Dupont and Alley, 2005). However, these ice shelves are increasingly vulnerable to disintegration due to a mix of factors, including atmospheric-driven surface melt (van den Broeke, 2005; Lenaerts et al., 2017), ocean-driven basal melt (Pritchard et al., 2012), and loss of structural integrity from ocean forcing (Wilmes et al., 2017; Massom et al., 2018) and surface velocity differences (Lhermitte et al., 2020). While surface melt has played a marginal role in the past (Rignot et al., 2019), it is becoming more important to the Antarctic Ice Sheet's fate as temperatures continue to rise (Gilbert and Kittel, 2021; Trusel et al., 2015; van Wessem et al., 2023). Therefore, it is essential to closely monitor surface melt on Antarctic ice shelves to better comprehend and anticipate climate change impacts.

Satellite remote sensing enables long-term and frequent mapping of the extent and dynamics of surface meltwater over the Antarctic ice shelves. Microwave remote sensing is particularly suited for this purpose because microwave signals are very sensitive to liquid water, and observations can be acquired even during cloudy conditions or at night (de Roda Husman et al., 2022). Microwave remote sensing

* Corresponding author.
E-mail address: S.deRodaHusman@tudelft.nl (S. de Roda Husman).

https://doi.org/10.1016/j.rse.2023.113950
Received 5 July 2023; Received in revised form 28 November 2023; Accepted 4 December 2023
Available online 8 December 2023

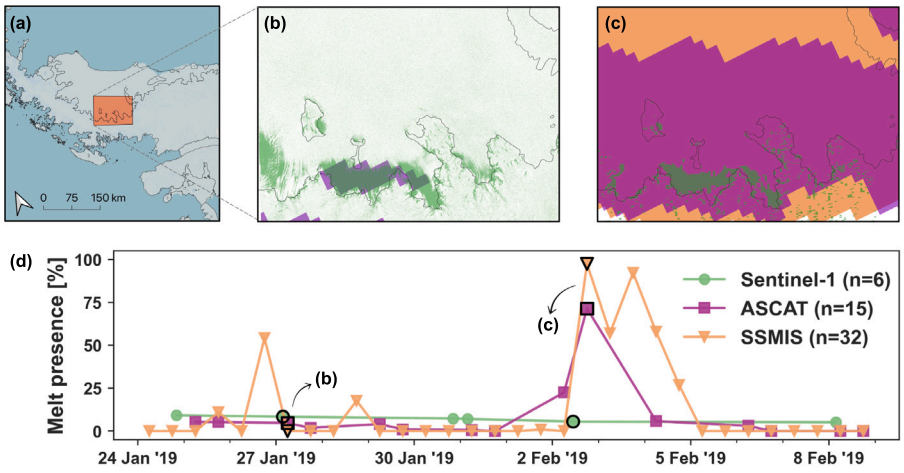

Fig. 1. Illustration of the temporal–spatial resolution trade-off for surface melt detection. A small part of the Larsen C Ice Shelf is selected as the area of interest, shown in (a). Spatial plots of detected surface melt by Sentinel-1 (green), ASCAT (purple), and SSMIS (orange) are presented for 27 January 2019 in (b) and 2 February 2019 in (c). Panel (d) displays a time series illustrating the percentage of pixels within the study region where melt was detected. Melt is determined using threshold-based melt detection algorithms, developed by Ashcraft and Long (2006) for Sentinel-1 and ASCAT, and by Zwally and Fiegles (1994) for SSMIS.

techniques can be separated into two classes: active microwave sensors, which measure backscatter intensity, i.e., the normalized radar cross-section (σ^0), and passive microwave sensors, which observe the brightness temperature (T_b) (Ulaby and Long, 2014). When melting starts, the emissivity and absorptivity of snow and ice increase significantly because of the abrupt increase of the dielectric constant, leading to a sudden decrease in backscatter intensity and an increase in brightness temperature (Ashcraft and Long, 2006; Liu et al., 2006).

Many recent studies have developed methods to detect surface meltwater over the Antarctic ice shelves using active or passive microwave satellite data (e.g., Trusel et al., 2012; Mousavi et al., 2022; Johnson et al., 2020). Even though these methods have shown widespread surface melt over the Antarctic ice shelves, detecting melt using data from a single satellite has limitations (see Fig. 1). Microwave sensors such as Special Sensor Microwave Imager/Sounder (SSMIS) and Advanced Scatterometer (ASCAT) cover the entire Antarctic Ice Sheet at a high, twice-daily temporal resolution. Nevertheless, their coarse, kilometer-scale spatial resolutions are insufficient to observe small-scale melt features, such as complex surface melt patterns induced by topography at the grounding line (Lenaerts et al., 2018). Data from synthetic aperture radar (SAR) sensors, such as aboard Sentinel-1, can be obtained with a much finer, meter-scale spatial resolution but often miss melt events that occur only during short periods of time due to the low revisit time of the satellite (i.e., a few times per week).

Deep learning techniques provide a promising solution to tackle the trade-off between temporal and spatial resolution in satellite imagery. U-Nets (Ronneberger et al., 2015), in particular, have gained widespread recognition in various fields, including cryospheric research (e.g., Radhakrishnan et al., 2021; Mohajerani et al., 2019; Niu et al., 2023; van der Meer et al., 2023; Baumhoer et al., 2019). The aforementioned studies have showcased the ability of U-Nets to identify and capture spatial patterns, positioning them as a promising tool for effectively capturing the complex spatial melt patterns observed on Antarctica. Additionally, by processing data at frequent time intervals, U-Nets enable valuable insights into the duration, frequency, and evolution of melt events.

In this study, we present a U-Net to combine data from multiple microwave satellites into a high-resolution surface melt record, referred to as UMelt. In this way, we overcome specific sensor limitations, related to the trade-off between spatial and temporal resolution, which allows us to establish a record of surface melt over the Antarctic ice shelves at a high spatial (500 m) and high temporal (12 h) resolution for the period 2016–2021. The record is based on a combination of three microwave satellites with varying spatiotemporal resolutions, namely Sentinel-1, ASCAT, and SSMIS. Combining these data, the U-Net learned to recognize the fine-scale Sentinel-1 melt patterns, enabling the production of detailed melt maps from the coarse spatial resolution ASCAT and SSMIS observations, a digital elevation model (DEM), and multi-year Sentinel-1 melt fractions. In Section 2, the satellite and auxiliary data sets are introduced, and the training and validation of the U-Net are discussed. In Section 3, the performance of the model over training and testing ice shelves is presented, along with its application to all Antarctic ice shelves. The strengths and limitations of the developed U-Net are discussed in Section 4. The conclusion demonstrates how the high-resolution melt record can enhance our understanding of the impact of surface melt on Antarctic ice shelf stability in Section 5.

2. Materials and methods

2.1. Study area

We developed a U-Net to create UMelt, a high-resolution surface melt record for all Antarctic ice shelves. Like most deep learning algorithms, U-Nets require both training and testing data to effectively learn and make accurate predictions (Ronneberger et al., 2015). During the training phase, a U-Net is fed with a large data set consisting of input features (see Section 2.4.2) and their corresponding reference data (see Section 2.4.1), see Fig. 3. By exposing the U-Net to diverse training data, it becomes more capable of recognizing and generalizing spatial patterns in the data, allowing it to make informed predictions. After training, the U-Net's performance is evaluated using a separate set of testing data that it has never encountered before. This helps assess its ability to accurately segment unseen images.

Our U-Net model was trained on the Shackleton Ice Shelf, and subsequently tested on both the Shackleton and Larsen C ice shelves. The Shackleton Ice Shelf, a large ice shelf fronting the coast of East Antarctica, was selected as a training region based on three main factors. First, the Shackleton Ice Shelf has the most 'matching overpasses' (Fig. 2a), where Sentinel-1, ASCAT, and SSMIS overpasses were acquired with less than two hours difference. These 'matching overpasses' ensure comparable melt patterns between Sentinel-1, ASCAT, and SSMIS (see Section 2.5 for an elaborate description). Secondly, Saunderson et al. (2022) identified nine different melt patterns on the Shackleton Ice Shelf, which exhibited significant variability in the timing and spread of surface melt. This large variability in melt patterns on the Shackleton Ice Shelf provides a diverse and representative training data set for the U-Net model. Finally, the Shackleton Ice Shelf experiences substantial surface melting, averaging between 100–200 mm w.e. per year (Trusel

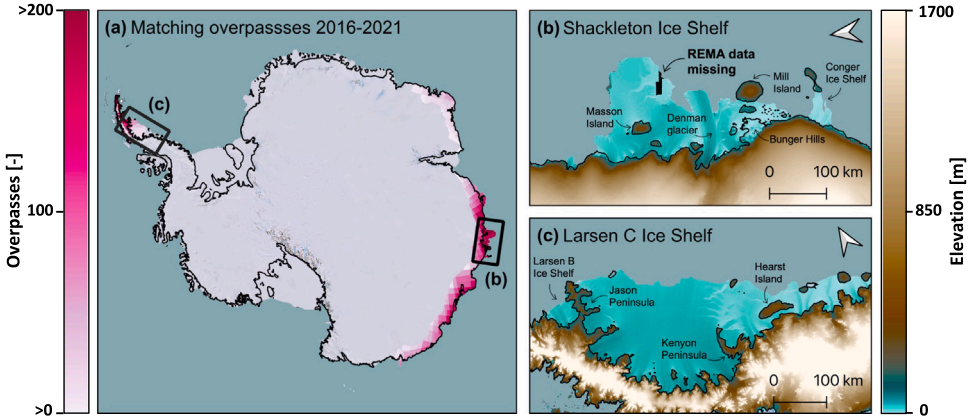

Fig. 2. The number of 'matching overpasses' in (a), indicating instances where the time difference between Sentinel-1, ASCAT, and SSMIS overpasses is less than two hours. The elevations of the training and testing regions, namely the Shackleton and Larsen C ice shelves, are depicted in panels (b) and (c). The Shackleton Ice Shelf has a small data gap, as indicated by the label "REMA data missing". Other labels on the map indicate various place names on the ice shelves.

et al., 2013). Among Antarctic ice shelves, it ranks as one of the most susceptible to surface melting, except for those located on the Antarctic Peninsula (Gilbert and Kittel, 2021; Trusel et al., 2013). Consequently, the peak melting months (December to February) closely mirror the melt patterns and corresponding remote sensing signals seen on the ice shelves with relatively high surface melt. Conversely, the months marking the beginning and end of the melting season (i.e., November and March) align with ice shelves that experience less frequent surface melting.

We tested the U-Net on the Larsen C Ice Shelf, which yielded valuable insights into the performance of the trained U-Net for three primary reasons. First, the geographic location of the two ice shelves on opposite sides of the Antarctic Ice Sheet meant that different melt patterns were expected, allowing for a robust assessment of the U-Net's transferability (i.e., the ability to apply knowledge gained from the training region to other regions without significant loss in performance). Secondly, the topography of the two ice shelves is markedly different. Large parts of the Shackleton Ice Shelf are surrounded by the ocean and buttressed by several ice rises, while the Larsen C Ice Shelf is mostly confined by land ice and has a more homogeneous elevation over its center but a notably steep grounding line (Fig. 2b and 2c). Finally, a more practical consideration was that, with around 50 'matching overpasses' over the Larsen C Ice Shelf, a sufficiently large testing data set was available to evaluate the U-Net's performance.

After training and testing, the U-Net model was applied on all Antarctic ice shelves between 2016 and 2021 to generate an Antarctic-wide high-resolution surface melt record: UMelt. Because there are (almost) no 'matching overpasses' for most of the Antarctic ice shelves (Fig. 2a), the accuracy of our UMelt record was only determined for the Shackleton and Larsen C ice shelves.

2.2. Melt masks

2.2.1. UMelt mask

Our UMelt record is available on a large part of the Antarctic Ice Sheet, but we have excluded some areas. The considered area of interest, referred to as the "UMelt mask", is provided in Supplementary Figure 1a. First, extensive parts of the interior of the Antarctic Ice Sheet where high accumulation rates result in a low backscatter intensity (around −15 dB) were omitted, following the approach of Zheng and Zhou (2020). Under such conditions, surface melt detection algorithms may classify pixels erroneously as surface melting, whereas no surface melt has been observed on the interior of the ice sheet (e.g., Van Wessem et al., 2018). Moreover, pixels with an elevation over 1700 m were ignored, as surface melt is unlikely to occur there (Banwell et al., 2021; de Roda Husman et al., 2022). Finally, areas with no Sentinel-1 overpasses were removed (refer to Figure 2 in de Roda Husman et al. (2022)), because we were unable to generate the multi-year Sentinel-1 melt fraction input feature. After implementing these exclusions, the study area was reduced to 1.8 million km^2, which accounts for 12.7% of the total area of the Antarctic Ice Sheet.

2.2.2. U-Net development mask

To test and train the U-Net model, we excluded additional regions beyond those covered by the UMelt mask (described in Section 2.2.1). Specifically, we omitted damaged regions, which are known to confuse melt detection algorithms on the reference product, Sentinel-1 (Zhou et al., 2019; Dirscherl et al., 2021). Damaged regions, i.e., regions containing fractures, rifts, or crevasses on the ice surface, lead to distortions in SAR images. These distortions result in high backscatter intensities for slopes facing towards the sensor (known as radar foreshortening) and low backscatter intensities for slopes facing away from the sensor (known as radar shadows). These radar shadows can be mistakenly identified as surface melt. Therefore, we created a "damage mask" using the damage detection method developed by Izeboud and Lhermitte (2023). This method detects the presence of a fracture feature within a group of pixels based on a line detection algorithm. Noise is removed using a sensor- and processing-resolution specific threshold, for which we used $\tau = 0.1$ (damage detection applied to Sentinel-1 EW images, processed on 100 m resolution with 10 × 10 pixel groups). Furthermore, a buffer with a radius of 5 km was applied to mask neighboring pixels.

In comparison to the UMelt mask (Section 2.2.1), removing the damage pixels for the Shackleton Ice Shelf resulted in an 8% reduction, transforming the UMelt mask from 52×10^3 km^2 to a UMelt development mask of approximately 48×10^3 km^2. Similarly, for the Larsen C Ice Shelf, about 9% of pixels were removed from the UMelt mask to derive the UMelt development mask, decreasing from 84×10^3 km^2 to 77×10^3 km^2.

2.3. U-Net architecture

We used an "Attention U-Net" architecture for our image segmentation task, which is an extension of the traditional U-Net (Ronneberger et al., 2015) that incorporates attention gates to selectively highlight relevant features (Oktay et al., 2018; Trebing et al., 2021). Our network consisted of two main parts: the contracting path for encoding and the expansive path for decoding (see Fig. 3).

In the contracting path, the input features were progressively downsampled by convolutional layers and max-pooling operations, allowing the network to extract high-level features (Girshick et al., 2014). These high-level features capture information about the rough outlines of surface melt events, disregarding small-scale melt details. These features

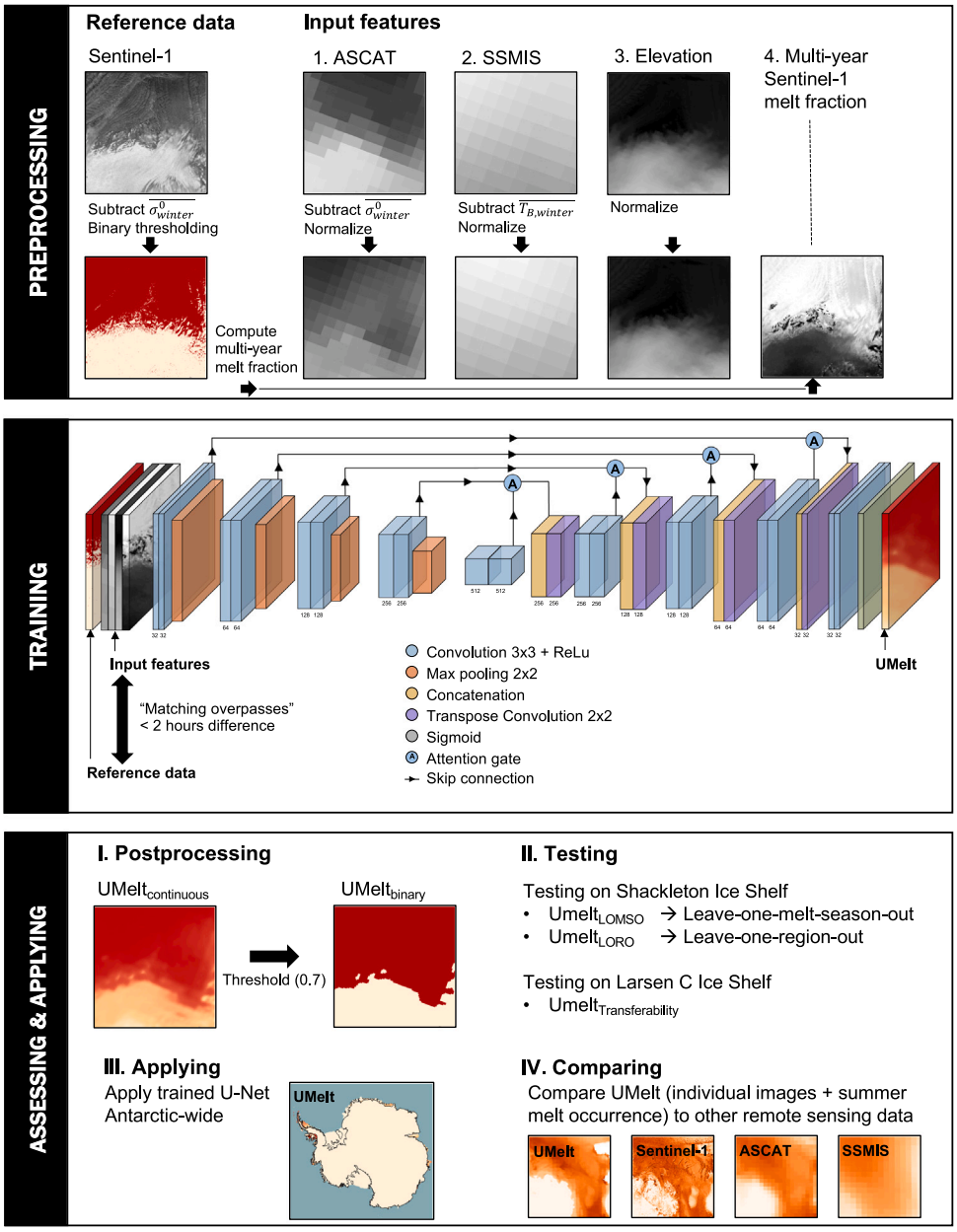

Fig. 3. Conceptual overview of the method employed in this study, which is divided into three key steps: preprocessing, training, and assessing & applying. The details of this method are discussed in Sections 2.4–2.7.

are analogous to the large-scale melt patterns observed by Saunderson et al. (2022), who studied surface melt using satellite data with a 25 km spatial resolution on the Shackleton Ice Shelf. In the expansive path, the features coming from the encoder are upsampled by transposed convolutions. Furthermore, they are concatenated with features from the contracting path through skip connections, which connect corresponding encoder and decoder layers. This preserves low-level features, such as the spatial arrangements of melt pixels on a small scale. The attention gates were added to these skip connections to allow the network to selectively focus on important features while filtering out irrelevant information (Oktay et al., 2018).

We conducted hyperparameter tuning on the validation data set (See Section 2.5) to optimize the performance of our Attention U-Net model. We did a grid search over all possible combinations of hyperparameters (Bengio, 2012), which included the learning rate (0.05, 0.01, 0.005, 0.001, 0.0005, 0.0001), batch size (16, 32, 64, 128), the number of filters for the first layer, which was doubled in each subsequent layer (16, 32, 64, 128), and the dropout rate (constant rate of 0.5 applied to the different convolution layers). For each combination of hyperparameters, we trained the model on the training data set and evaluated its performance (i.e., segmentation accuracy) on the validation data set to identify the optimal configuration. The optimal hyperparameters maximized the segmentation accuracy (learning rate: 0.001; batch size: 32; number of channels: 32; dropout rate of 0.5: applied to the fourth and fifth convolution layers). In cases where the difference in validation accuracy was less than 1% for different hyperparameters, we selected the most computationally efficient ones.

We employed commonly used and standard algorithms for activation, loss, and optimization, which are (almost) similar to those employed in previous works such as Dahle et al. (2022), Mastrofini et al. (2023), and Zhao et al. (2022). Specifically, the Rectified Linear Unit (ReLU) activation function was utilized for the hidden layers, effectively eliminating negative values within the neural network and allowing only positive values to propagate. Additionally, the sigmoid activation function, commonly employed in binary classification tasks, was employed in the final layer to compress the output within the range

of 0 to 1, representing the probability. To address the class imbalance issue in the training data, where non-melt pixels outnumbered melt pixels by a factor of four, we incorporated class weighting based on the melt and non-melt pixels ratio into the binary cross-entropy loss function. This ensured that missing a surface melt event incurred a higher penalty compared to missing a non-melt event. The Adam optimization algorithm was used, which allowed efficient training and parameter optimization.

The model was trained for a maximum of 30 epochs, with each epoch taking approximately 10 min. Early stopping was implemented to stop training when the validation loss did not improve for three consecutive epochs. The default early stopping settings were used, considering any improvement, regardless of magnitude, as progress. As a result, the U-Net model used for generating the UMelt record was trained for 10 epochs. However, for other models used to evaluate spatial and temporal performance, the number of epochs varied between 5 and 12.

To perform the training, we utilized Google Colab, a cloud-based platform that offers GPU access for deep learning tasks. TensorFlow, the deep learning framework used to code our model, is integrated into Google Colab, simplifying the process of building and training the model.

2.4. Preprocessing

2.4.1. Reference data

Sentinel-1 observations were used to create the reference data (sometimes referred to as target or ground truth data) for the U-Net. We used Sentinel-1 Level-1 Ground Range Detected (GRD) scenes in the linear scale that were preprocessed in the Google Earth Engine (Gorelick et al., 2017). This preprocessing included orthorectification, radiometric calibration, thermal noise removal, and border noise removal. It is worth noting that border noise removal was applied to scenes from January 2018 onwards in the preprocessed images available in the Google Earth Engine. This occasionally leads to noisy pixels at the edges of scenes prior to January 2018.

We selected all available horizontally polarized GRD scenes over the Antarctic Ice Sheet for melt seasons 2016–2021, allowing a combination of Interferometric (IW) and Extra Wide (EW) overpasses. The scenes were resampled to a 500 m resolution using bilinear interpolation and reprojected to WGS 84 Antarctic Polar Stereographic projection (EPSG:3031). The utilization of a 500 m spatial resolution enabled the detection of surface melt features at a small scale, while concurrently ensuring the data could be processed efficiently.

Then, we derived the binary melt presence (i.e., melt/non-melt) for the Sentinel-1 observations using the widely used melt detection algorithm proposed by Ashcraft and Long (2006). Melt presence was assumed when the backscatter intensity was smaller than the annual winter mean minus a certain threshold by using the following equation:

$$m(t) = \begin{cases} 1, & \sigma^0(t) < \sigma^0_{winter} + \Delta\sigma^0 \\ 0, & \sigma^0(t) \geq \sigma^0_{winter} + \Delta\sigma^0 \end{cases} \quad (1)$$

where σ^0_{winter} is the average backscatter intensity of the previous winter months, and $\Delta\sigma^0$ is the threshold which was set to −3 dB (similar to Ashcraft and Long, 2006). To address the substantial disparities in backscatter intensity across different orbits, we implemented Eq. (1) on a per Sentinel-1 orbit basis. This approach accounts for the variations in backscatter intensities stemming from differences in incidence angles.

2.4.2. Input features

The U-Net input received four input features: ASCAT, SSMIS, elevation, and the multi-year Sentinel-1 melt fraction (see Fig. 3), offering diverse information related to surface melt patterns and characteristics. ASCAT, similar to Sentinel-1, is an active microwave satellite. However, it exhibits lower spatial resolution (kilometer-scale instead of meters) and a higher revisit time (twice a day instead of a few times per week) when compared to Sentinel-1. Consequently, we expect that ASCAT will provide valuable information on the dynamic changes in melt patterns over time, although it may primarily capture coarse-scale patterns. Similar to ASCAT, SSMIS also provides information on liquid water presence on a coarse spatial scale but with a high temporal resolution. However, it is important to consider that SSMIS measures the brightness temperature instead of the backscatter intensity. This distinction means that SSMIS is influenced by various parameters beyond just liquid water content, which can result in significant differences in large-scale patterns compared to Sentinel-1 and ASCAT (Mote and Anderson, 1995; Hofer and Mätzler, 1980). Nevertheless, SSMIS is highly sensitive to detecting even small amounts of liquid water, enabling valuable insights into less intense melt events (Picard et al., 2022). The role of elevation data is also crucial in this study, given its high spatial resolution and well-established inverse correlation with melt patterns (Trusel et al., 2013). In addition to the aforementioned input features, multi-year melt fractions from Sentinel-1 are also utilized to provide insights into spatial details. Although these details may not be critical for capturing day-to-day variations, which are significant in Antarctica, they offer valuable information about the most common fine-scale melt patterns. The subsequent paragraphs will sequentially elaborate on the details of the four input features.

For the ASCAT input feature, we utilized vertically polarized observations with a 4.45 km resolution, consistent with prior studies (e.g., Trusel et al., 2012; Bevan et al., 2018; de Roda Husman et al., 2022), obtained from the Brigham Young University Microwave Earth Remote Sensing Laboratory (www.scp.byu.edu). ASCAT captures observations of the Antarctic Ice Sheet every other day at 6 AM (morning) and 6 PM (evening). We calculated averages to address days without observations by combining the morning before and after a missing morning observation (and similarly for missing afternoon observations). This process allowed the creation of a twice-daily ASCAT time series. Then, instead of generating binary melt presence from ASCAT observations by applying a threshold (i.e., $\Delta\sigma^0$ in Eq. (1)), we only subtracted σ^0_{winter} from the ASCAT observations. Continuous data carry more information than binary data, allowing the U-Net to learn the most appropriate threshold depending on the situation rather than relying on a specific threshold value. Finally, we normalized these values between the low (5th percentile) and high (95th percentile) values of ASCAT minus the winter mean over the Shackleton Ice Shelf for the melt seasons from 2016–2021, without capping values below zero or larger than one.

We utilized horizontally polarized 19 GHz SSMIS observations from the NASA MEaSUREs project (Brodzik et al., 2016) as the second input feature, with a spatial resolution of 6.25 km (similar to, e.g., Wang et al., 2022b; Wei et al., 2022). Observations from the F17 sensor were selected, which consistently passed over at approximately 6 AM and 6 PM during our study period. We applied a similar approach as for ASCAT and created continuous and normalized melt observations by subtracting the average brightness temperature of the previous winter months and scaling the values between the 5th and 95th percentiles.

As for the third input, we utilized the Reference Elevation Model of Antarctica (REMA) mosaic to inform the model on the elevation of the Antarctic Ice Sheet (Howat et al., 2019). The REMA mosaic has a high resolution of two or eight meters, depending on the location. For this study, the resampled version with a resolution of 200 m was used, which was sufficient for our purposes. While the REMA mosaic provides extensive coverage of the continent, there are some gaps in coverage, including a small area of the Shackleton Ice Shelf (as shown in Fig. 2b). We disregarded the data gaps, predominantly located along the edges of ice shelves with minimal surface melt.

The fourth input feature consisted of the multi-year melt fractions of Sentinel-1 data, derived from the reference data discussed in Section 2.4.1. The multi-year Sentinel-1 melt fractions were computed by summing the monthly melt pixels obtained using Eq. (1) and then dividing the sum by the total number of observations in that specific month. We are aware that using Sentinel-1 as reference and input

data may raise concerns about information leakage. To address this, we ensured the exclusion of the month of interest from the calculation, aiming to eliminate any potential correlation between the input features and reference data. For instance, when calculating the multi-year melt fraction for November 2016, the melt fraction was derived from the November months of 2017 until 2021. To validate that the U-Net model was not simply replicating the monthly melt fractions of Sentinel-1, we conducted an assessment of the importance of each feature, as described in Section 2.7.

Finally, the four input features were resampled to match the scale and projection of the preprocessed Sentinel-1 scenes, which were in the WGS 84 Antarctic Polar Stereographic projection with a resolution of 500 m.

2.4.3. Comparison UMelt to Sentinel-1, ASCAT, and SSMIS

To facilitate a comparison between the UMelt record and surface melt observations from Sentinel-1, ASCAT, and SSMIS, binary melt products were also derived from ASCAT and SSMIS observations. The approach used for Sentinel-1 was explained in Section 2.4.1, while continuous values were utilized as input for ASCAT and SSMIS (as described in Section 2.4.2). A further step was required to compare these data with the UMelt record: converting the continuous ASCAT and SSMIS data to binary melt estimates using thresholding algorithms. We applied the same melt detection algorithm used for Sentinel-1 (Eq. (1)) to ASCAT to achieve this. For SSMIS, a melt detection algorithm suggested by Torinesi et al. (2003) was implemented, which has been used in several previous studies (e.g., Wille et al., 2019; Banwell et al., 2021; Johnson et al., 2020). The algorithm defines surface melt based on the observed brightness temperature surpassing an empirical threshold, typically between 30 K and 40 K. This dynamic threshold is determined using the mean and variability of the brightness temperatures recorded during the preceding winter.

In addition to comparing UMelt with single observations from Sentinel-1, ASCAT, and SSMIS, we calculated the "summer melt occurrence" following the methodology of de Roda Husman et al. (2022). The summer melt occurrence, computed for each melt season spanning November through March, represents the ratio of the number of melt observations to the total number of observations per pixel. The metric is expressed as a percentage and was computed using binary products obtained from UMelt, Sentinel-1, ASCAT, and SSMIS.

2.5. Training, validation, and testing data

The training, validation, and testing data were selected according to the criterion that the temporal difference in Sentinel-1, ASCAT, and SSMIS overpass times was less than two hours. This criterion was important as surface melt can occur for a very short duration, and larger differences in overpass time may lead to disparities in the detected surface melt among the satellite observations. The 'matching overpasses' of Sentinel-1, ASCAT, and SSMIS were then combined with the elevation and Sentinel-1 multi-year melt fraction data sets, creating a 5-band (i.e., channels) image comprising reference labels (i.e., Sentinel-1 binary melt) and four input features (i.e., ASCAT, SSMIS, elevation, and multi-year Sentinel-1 melt fraction).

We employed stratified sampling to achieve a balanced data set for effective learning and recognition of melt patterns by the U-Net model. This process involved randomly selecting points on the Shackleton Ice Shelf, all within the U-Net development mask (Supplementary Figure 1b). For each 'matching overpass', a total of 10 points were selected, comprising an equal number of melt pixels (5) and non-melt pixels (5), determined by the Sentinel-1 labels. It is worth noting that only non-melt pixels were selected if a Sentinel-1 scene did not contain any melt pixels. Subsequently, we generated patches of input features and labels by selecting neighboring pixels around the sampled points. As the stratified sampling points were randomly distributed, patches could overlap. Each patch was sized at 64 × 64 pixels, equivalent to 32 × 32 km, ensuring they captured sufficient detail to represent the melt patterns accurately and guaranteeing an appropriate distribution of melt locations. Finally, all patches from one 'matching overpass' were assigned to either the training data set (80%), the validation data set (10%), or the testing data set (10%). Each set's approximate number of pixels was 15 million for training, 2 million for validation, and 2 million for testing.

2.6. Post-processing

After training the U-Net, the model was applied to create the UMelt record. We stacked the input features (i.e., ASCAT, SSMIS, elevation, and multi-year Sentinel-1 melt fraction) and tiled the data into patches of 64 × 64 pixels (similar to in Section 2.5), using an 8-pixel overlap on all sides. In overlap regions, prediction results were calculated as the mean of the prediction probabilities.

Next, we converted the prediction probabilities into a binary product using a threshold of 0.7. We determined that this specific threshold value yielded the best performance on the validation set (see Supplementary Figure 3). Pixels with probability values exceeding the 0.7 threshold were identified as melt pixels, whereas those below the threshold were labeled as non-melt.

2.7. Accuracy assessment

To assess the performance of our U-Net model, we utilized the test data set, which was not used during the training and validation phases. Several performance metrics, including precision, recall, F1-score, and accuracy, were calculated. Precision measures the fraction of true positive predictions among the total predicted positive instances, while recall measures the fraction of true positive predictions among the total actual positive instances. The F1-score is the harmonic mean of precision and recall, providing a single value that combines both measures. Accuracy measures the overall proportion of correct predictions over all instances.

Cross-validation is essential for training the U-Net model as it enables reliable performance evaluation, prevents overfitting, and improves our understanding of its effectiveness (Roberts et al., 2017; Bolibar et al., 2020). Specifically, to assess the temporal performance of the U-Net, we performed a 'leave-one-melt-season-out' (*LOMSO*) analysis. We evaluated the model's performance when applied to the melt season that was excluded from training. In Section 3, we discuss the accuracies over a very wet season (2019–2020), a very dry season (2020–2021), and an average melt season (2016–2017). High accuracies over unseen melt seasons hint at a good performance of the U-Net over other ice shelves with more or less extreme melt intensities than at the Shackleton Ice Shelf.

In order to evaluate the model's spatial performance, we partitioned the Shackleton Ice Shelf into four distinct parts with similar areas (see Supplementary Figure 1d). Then, we implemented a 'leave-one-region-out' (*LORO*) approach to assess the model's accuracy when applied to an unseen region. The melt patterns are very diverse over the ice shelf. Therefore, a high accuracy over an unseen region means the model is probably well-capable over other Antarctic ice shelves.

We assessed the transferability of the U-Net by applying the model to the Larsen C Ice Shelf for melt season 2016–2017. We applied the trained model for which melt season 2016–2017 was excluded, so that we could assess the performance for both an unseen spatial and temporal domain. Please be aware that our model's transferability was exclusively evaluated over the Larsen C Ice Shelf. This is due to a lack of 'matching overpasses' on other ice shelves (see Fig. 2a). Consequently, accuracy computations for ice shelves other than Shackleton and Larsen C were hindered.

In the final stage of the accuracy assessment, the significance of the four input features was evaluated by training four separate models, with each model excluding one feature at a time. The training was

conducted over melt seasons 2017–2021, and the performance was assessed on the unseen melt season 2016–2017. By comparing the accuracies and spatial patterns of these models, we could determine the importance of each input feature. If a model exhibited notably lower performance compared to the model utilizing all four features, it indicated the excluded input feature's significance.

3. Results

We evaluated the performance of the U-Net model using varying spatial and temporal domains of the training, validation, and testing data sets. We present the results over the Shackleton Ice Shelf, Larsen C Ice Shelf, and Antarctic-wide in Sections Section 3.1, 3.2, and 3.3, respectively. Supplementary Table 1 contains the accuracy assessment results for all experiments.

3.1. Surface melt over Shackleton Ice Shelf

3.1.1. Temporal performance

We first evaluated the performance of the U-Net model on the Shackleton Ice Shelf in terms of temporal performance. Specifically, we examined the model's ability to predict melt events during unseen seasons, which we refer to as UMelt_{LOMSO}. Fig. 4 shows that UMelt_{LOMSO} performed well on three distinct days at the beginning, middle, and end of the 2016–2017 melt season, despite not being trained on data from the 2016–2017 season (see Supplementary Video 1 for melt observations for all days with 'matching overpasses'). The model accurately identifies the complex melt patterns over the Shackleton Ice Shelf, resulting in an F1-score of 86.9% and an accuracy of 91.3% when compared to Sentinel-1. Notably, ASCAT and SSMIS (Fig. 4, column 4 and 5, respectively) detect mostly larger melt patterns, with the exception of the western part of the Shackleton Ice Shelf. Here, SSMIS tends to underestimate melt due to the presence of a frequently-occurring polynya that results in lower brightness temperatures, as noted by Nihashi and Ohshima (2015). However, both sensors often miss the detailed melt patterns captured by the reference product Sentinel-1. Our UMelt product is well able to detect these small-scale patterns, especially along the grounding line and on Masson Island (location indicated in Fig. 2).

The accuracy of UMelt, ASCAT, and SSMIS melt observations compared to the reference product Sentinel-1 is displayed in Fig. 4d. UMelt achieved an average accuracy of 91.3% for the 2016–2017 melt season, which is higher than the average accuracies of ASCAT and SSMIS, with 90.0% and 82.3%, respectively.

UMelt is particularly effective in detecting small-scale patterns, such as those found on the grounding line and on Masson and Mill islands (Fig. 5). In contrast, ASCAT and SSMIS incorrectly detect melt at Masson Island (Fig. 5f), where the elevation is over 1000 m and Sentinel-1 does not indicate any surface melt. In addition, Sentinel-1 shows a wide range of melt patterns over the grounding line (Fig. 5e and i), which UMelt_{LOMSO} accurately simulates. The detected melt on the Bunger Hills (Fig. 5h) demonstrates the most notable difference, with Sentinel-1 revealing complex melt patterns, while ASCAT and UMelt show minimal detection of melt. In contrast, SSMIS detects melt throughout the entire Bunger Hills region but lacks the expected level of detail considering the diverse terrain and varying elevations.

Additionally, our findings indicate that UMelt outperformed ASCAT and SSMIS for the 2019–2020 and 2020–2021 melt seasons (Supplementary Figure 2). In the 2019–2020 melt season, UMelt obtained an average accuracy of 90.9%, while in the 2020–2021 melt season, it achieved a higher accuracy of 95.7%. However, it is important to note that the F1-score for the 2020–2021 melt season was significantly lower (33.5%) than that of the 2016–2017 (86.9%) and 2019–2020 (82.7%) melt seasons. The 2020–2021 melt season experienced minimal melting, which is clearly reflected in the cumulative yearly melt maps by Picard (2022) (more details on the melt maps in Picard and Fily, 2006). Out of the small amount of melt that did occur, only 55.3% of the identified melt pixels were accurately classified.

3.1.2. Spatial performance

The model also showed a solid performance when regions of the ice shelf were not included during training, as shown in Fig. 6. In particular, we found that for the two regions located at the center of the ice shelf (Region 1 and Region 3), the accuracies of UMelt trained on all regions and UMelt_{LORO} were comparable, with an average difference in accuracies of 0.3% and 0.4%, respectively. However, Region 3 resulted in the lowest accuracy of the four regions, both for UMelt (i.e., 87.6%) and UMelt_{LORO} (i.e., 87.2%), whereas all the other regions resulted in accuracies exceeding 90%.

In the case of Regions 2 and 4, which are situated at the grounding line, we observed similar discrepancies in accuracy between UMelt and UMelt_{LORO} as for Regions 1 and 3, ranging from 0.2–0.4%. However, when examining specific pixels along the grounding line, UMelt_{LORO} exhibited over- or underestimation of surface melt occurrence by -25% to +25% compared to UMelt. In general, UMelt predicts a melt presence further inland, whereas the melt presence predicted by UMelt_{LORO} for Regions 2 and 4 ends closer to the grounding line. However, it comes as no surprise that the most significant discrepancy is evident along the grounding line. This region showcases exceptionally intricate melt patterns that ASCAT and SSMIS struggle to resolve adequately because of their limited spatial resolution. Despite this, the comparable performance of UMelt and UMelt_{LORO} is promising for the application of UMelt on an Antarctic-wide scale, showcasing that the U-Net demonstrates favorable performance even on untrained regions.

3.1.3. Feature importance

Convolutional neural networks are black-box algorithms, and their lack of transparency regarding feature importance remains a challenge (Olden and Jackson, 2002). However, we can get an estimate of the importance of features by iteratively removing them during the training of the model and evaluating its performance (Zhang et al., 2018).

Fig. 7 demonstrates the importance of the four input features used for the development of UMelt: ASCAT, SSMIS, elevation, and multi-year Sentinel-1 melt fraction. The results show that ASCAT is the most important feature, as evidenced by the drop in accuracy from 91.3% to 80.2% when ASCAT is removed from the training phase (Supplementary Table 1). The exclusion of ASCAT reduces surface melt across the entire study area, emphasizing its significance as an input feature. This is not surprising as both ASCAT and the reference data Sentinel-1 are C-band active microwave sensors, and therefore result in melt patterns that are comparable on a larger scale (although smaller details may differ due to spatial resolution differences).

In contrast, SSMIS, elevation, and multi-year Sentinel-1 melt fraction are less important, and their exclusion results in comparable disagreement with Sentinel-1 as the model trained on all input features (Supplementary Table 1). However, including these features results in the identification of detailed melt patterns similar to those in Sentinel-1. Additionally, multi-year Sentinel-1 melt fraction is important for melt detection on the eastern part of the Shackleton Ice Shelf (Fig. 7e), where small surface lakes are present annually (Arthur et al., 2020), but are not detected by ASCAT and SSMIS due to their low spatial resolution.

3.2. Surface melt over Larsen C Ice Shelf

In order to ensure that the U-Net model is applicable on an Antarctic-wide scale, we assessed its performance on the Larsen C Ice Shelf during the 2016–2017 melt season. We applied the UMelt_{LOMSO}, which was trained on the Shackleton Ice Shelf for the melt seasons between 2017–2021. This provides a fully out-of-sample performance estimate of our model since the trained model has neither seen the spatial region nor the temporal period of the target data set.

The general melt patterns from UMelt on Larsen C overlap well with the Sentinel-1 patterns, showing most melt in the western part of the

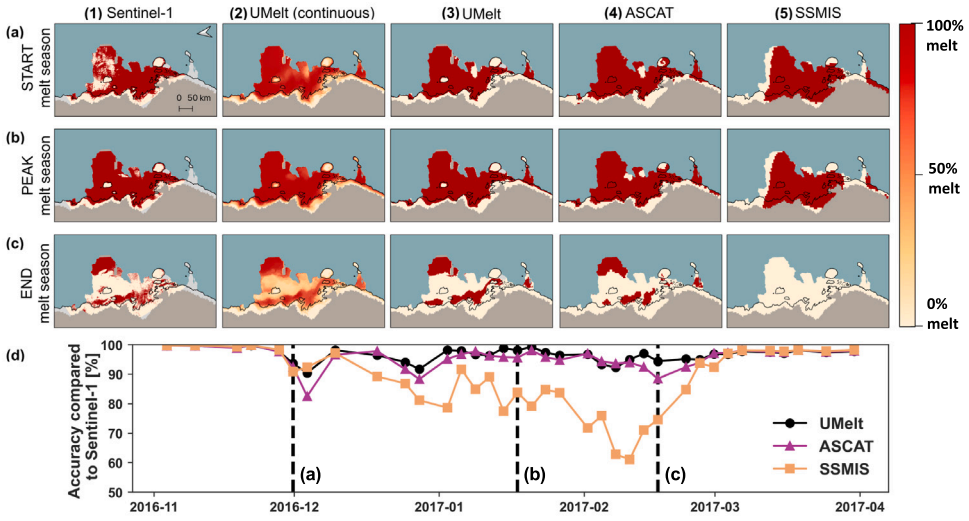

Fig. 4. The maps in (a), (b), and (c) present a comparison of reference data Sentinel-1 (first column) and our UMelt$_{LOMSO}$ product, visualized in both continuous format without threshold (third column) and binary format with a 0.7 threshold (second column), ASCAT (fourth column), and SSMIS (fifth column), at the beginning (30 November 2016, 6 PM), peak (17 January 2017, 6 PM), and end (16 February 2017, 6 PM) of the melt season of 2016–2017. The time series in (d) present the melt accuracy of UMelt (black), ASCAT (orange), and SSMIS (pink) compared to Sentinel-1 for melt season 2016–2017 on the Shackleton Ice Shelf.

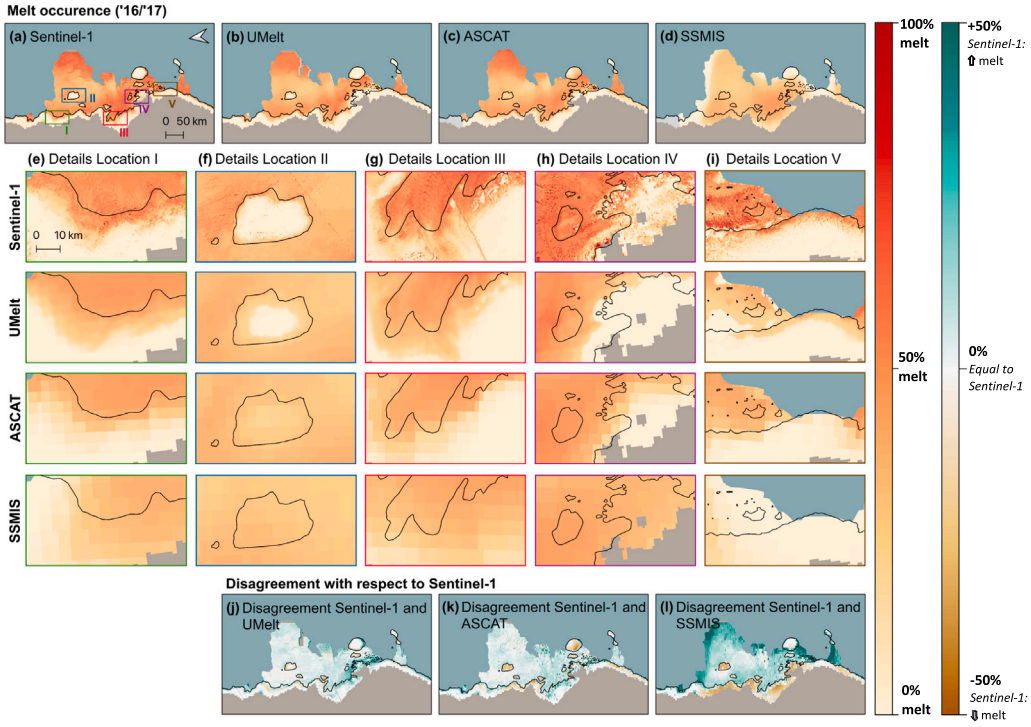

Fig. 5. The summer melt occurrence on Shackleton Ice Shelf for testing melt season 2016–2017 for Sentinel-1 (a), UMelt (b), ASCAT (c), and SSMIS (d). Details of five locations are shown in (e-i). The disagreements between Sentinel-1 and UMelt, Sentinel-1 and ASCAT, and Sentinel-1 and SSMIS are shown in (j-l).

ice shelf. However, in Figs. 8d and 8g, UMelt tends to overestimate surface melt landward of the grounding line where the elevation rapidly increases. There are two plausible explanations for this overestimation. First, the multi-year Sentinel-1 melt fraction, which is one of the input features, was derived from melt seasons spanning 2017 to 2021. During this period, surface melt was present landward of the grounding line. Hence, certain sections of the grounding line experienced an overestimation of surface melt during the 2016–2017 melt season, due to the comparatively wetter melt seasons observed between 2017 and 2021 (Bevan et al., 2020). Secondly, the Shackleton Ice Shelf, on which UMelt was trained, experiences surface melt at elevations up to around 300 m. The regions along Larsen C's grounding line where UMelt overestimated the surface melt are situated at elevations of 100–300 m, within the range where the UMelt model was trained to detect melting. Nevertheless, UMelt demonstrated a strong overall performance during the 2016–2017 melt season with an average F1-score of 89.3% with many UMelt patterns that matched with Sentinel-1. This is a better performance compared to Sentinel-1 than ASCAT and SSMIS, which have F1-scores of 85.9% and 80.0%, respectively.

3.3. Antarctic-wide surface melt

The U-Net was trained on the Shackleton Ice Shelf using data from all five melt seasons (i.e., 2016–2021) and subsequently applied to the

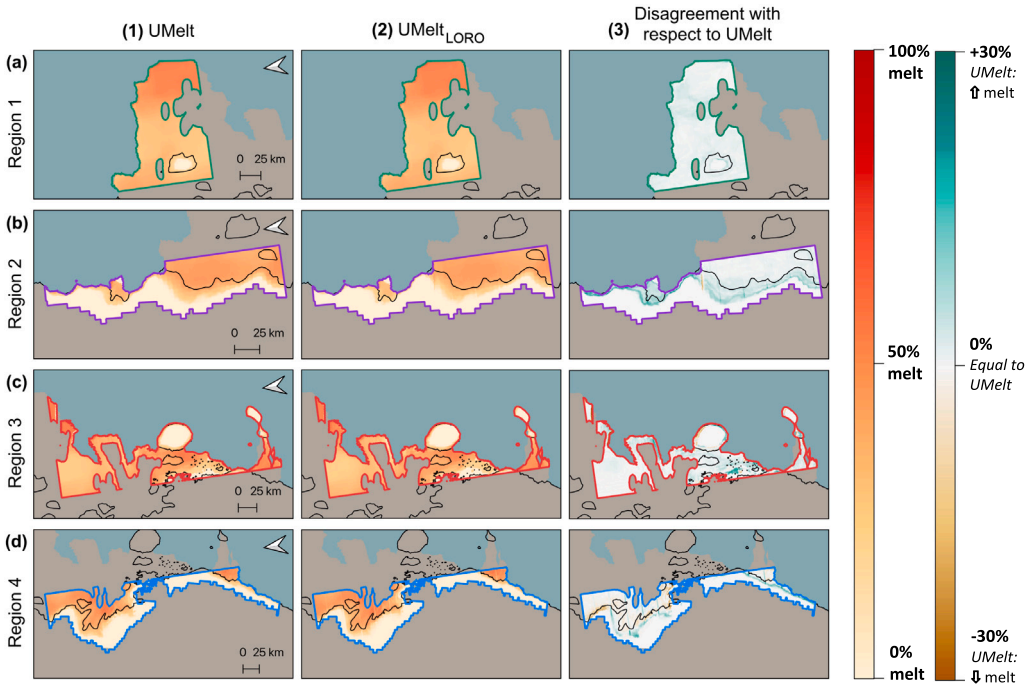

Fig. 6. Summer melt occurrence of UMelt (1) and UMelt$_{LORO}$ (2) for melt season 2016–2017 on the Shackleton Ice Shelf for the four leave-one-region-out (LORO) regions (a–d). UMelt (1) was trained on the entire ice shelf using data from melt seasons 2017–2021. UMelt$_{LORO}$ (2) was trained on the same period, but one region was excluded at a time. Then, the trained model was tested on the excluded region to evaluate the spatial transferability of the model. The disagreement between UMelt and UMelt$_{LORO}$ is shown in (3).

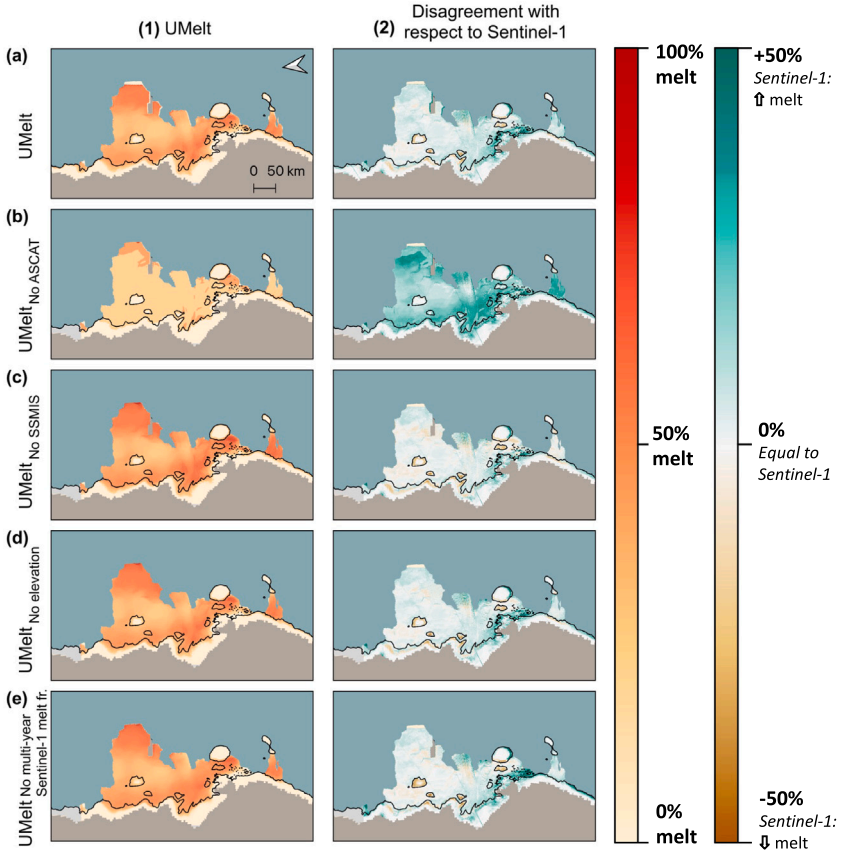

Fig. 7. Surface melt occurrence and performance compared to Sentinel-1 over the Shackleton Ice Shelf for the melt season 2016–2017 for different input features. Column 1 (a–e) displays the UMelt summer melt occurrence trained on different input features, where UMelt trained on all input features is presented in (a), and panels (b)–(e) correspond to UMelt with one of the input features excluded (ASCAT, SSMIS, elevation, and multi-year Sentinel-1 melt fraction, respectively). Column 2 (a)–(e) demonstrates the comparison of UMelt and Sentinel-1 performance, where the disagreements between Sentinel-1 and UMelt models trained with different input features are presented.

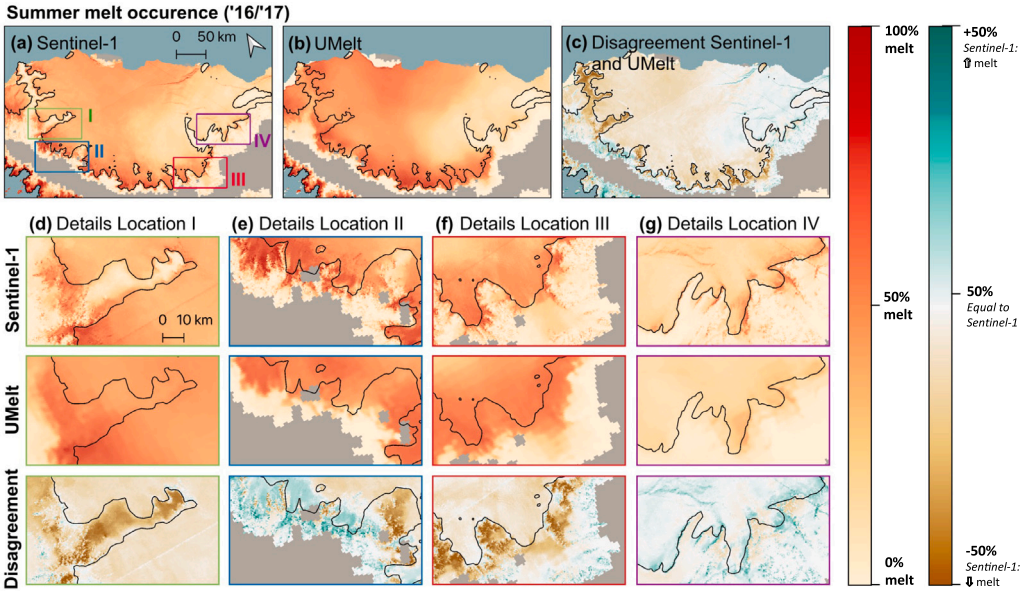

Fig. 8. The summer melt occurrence on Larsen C Ice Shelf for testing melt season 2016–2017 for Sentinel-1 (a), UMelt (b), and the disagreements between Sentinel-1 and UMelt (c). Details of four locations are shown in (d–g).

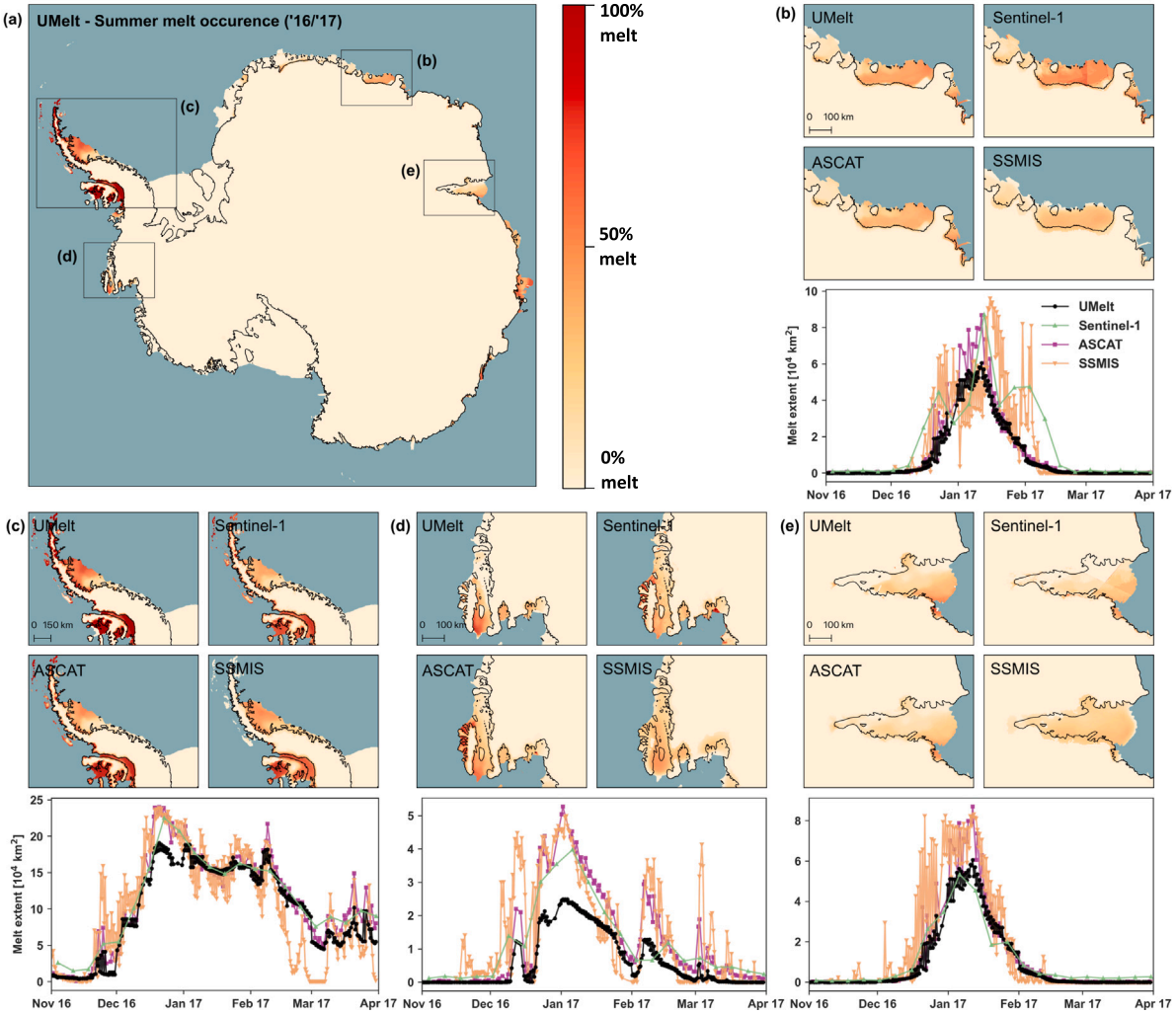

Fig. 9. The UMelt record, showing Antarctic-wide summer melt occurrence for melt season 2016–2017 (a), with details of Dronning Maud Land (b), the Antarctic Peninsula (c), Mary Byrd Land (d), and Amery Ice Shelf (e). The time series show a comparison in melt extent for the four regions between UMelt (black), Sentinel-1 (green), ASCAT (purple), and SSMIS (orange). (For interpretation of the references to color in this figure legend, the reader is referred to the web version of this article.)

entire Antarctic region, with the exception of the masked areas (see Section 2.2 and Supplementary Figure 1a), resulting in an observation area of 1.8 million km^2. The UMelt product for melt season 2016–2017 is presented in Fig. 9, while the summer melt occurrence derived from the melt observations of seasons 2017–2021 are shown in Supplementary Figure 4.

In the aggregated summer melt occurrence maps (Fig. 9), it becomes more difficult to identify the small-scale melt features captured by UMelt that were visible in earlier figures (Figs. 4, 5, and 6). However, almost all large-scale spatial melt patterns are consistent across UMelt, Sentinel-1, ASCAT, and SSMIS. Notably, the presence of melt in blue ice regions in the southeastern part of the Roi Baudouin Ice Shelf (Fig. 9b) and the western part of the Amery Ice Shelf (Fig. 9e) are only captured by the passive microwave satellite SSMIS. This discrepancy in detecting melt over blue ice areas is a recognized limitation of active microwave sensors (Zheng and Zhou, 2020; Zhou et al., 2019; de Roda Husman et al., 2022), including UMelt, which utilizes Sentinel-1 as the reference data. In the case of the Amery Ice Shelf (Fig. 9e), the Sentinel-1 summer melt occurrence map shows a clear boundary between areas with and without melt along the northern part of the grounding line. This distinction arises from the absence of Sentinel-1 observations in the northernmost region of the ice shelf during the 2016–2017 melt season. In the northern part of the Abbot Ice Shelf in Mary Byrd Land (Fig. 9d), UMelt successfully captures small-scale melt details that ASCAT and SSMIS are unable to capture. However, it is worth noting that UMelt tends to underestimate surface melt when compared to Sentinel-1, ASCAT, and SSMIS. Unfortunately, there are no 'matching overpasses' over Mary Byrd Land, including Abbot Ice Shelf, which prevents further evaluation of UMelt to Sentinel-1 in this region.

The time series plots in Fig. 9b–e illustrate the melt extent over the four regions throughout the 2016–2017 melt season. To account for the limited coverage of Sentinel-1, we created weekly aggregates representing the maximum melt extent. The time series analysis of Dronning Maud Land (Fig. 9b), Antarctic Peninsula (Fig. 9c), and Amery Region (Fig. 9e) reveals a close resemblance in total melt extent throughout the melt season among UMelt, Sentinel-1, ASCAT, and SSMIS. However, as we approach the conclusion of the melt season in Dronning Maud Land (Fig. 9b) and throughout the entire melt season in Mary Byrd Land (Fig. 9d), the time series indicate that UMelt tends to underestimate the extent of melt compared to the other sensors, especially compared to Sentinel-1 and SSMIS. It is crucial to take into account the restricted number of Sentinel-1 observations over Dronning Maud Land and Mary Byrd Land de Roda Husman et al. (2022). This means that the weekly averages are based on a limited data set, which may impact their reliability. The discrepancies with SSMIS could be attributed to the substantial difference in penetration depth between SSMIS and ASCAT/Sentinel-1 (Ulaby et al., 1986).

Fig. 9 demonstrates that UMelt serves as a viable alternative to existing satellite observations. In the context of high spatial resolution images of surface melt, Sentinel-1 observations have been commonly used (e.g., Liang et al., 2021). However, UMelt offers a significant advantage in terms of high temporal resolution. UMelt presents a notable advantage over Sentinel-1 by offering complete coverage without missing locations due to limited overpasses, a limitation observed in certain areas of the Amery Ice Shelf. Additionally, UMelt's twice-daily observation frequency eliminates the gaps in time that exist in Sentinel-1's time series.

Traditionally, sensors like ASCAT or SSMIS have been relied upon for high temporal resolution images (e.g., Bevan et al., 2018; Liu et al., 2006). However, their drawback lies in their low spatial resolution. In contrast, UMelt not only provides high temporal resolution but also captures spatial details that ASCAT and SSMIS fail to capture. Notably, UMelt reveals intricate features along the grounding lines of Larsen C and George VI ice shelves (Fig. 9c), as well as the western part of the grounding line on the Amery Ice Shelf (Fig. 9e). Therefore, UMelt proves to be a valuable tool in obtaining both detailed temporal and spatial information in melt observations, surpassing the limitations of Sentinel-1, ASCAT, and SSMIS.

4. Discussion

4.1. Opportunities of UMelt

The UMelt record demonstrates great potential as a new data product for surface melt monitoring, offering a viable alternative to existing remote sensing data sets such as Sentinel-1, ASCAT, and SSMIS. UMelt offers a significant advantage over ASCAT and SSMIS by effectively overcoming the limitations related to coarse spatial resolution while maintaining a high temporal resolution. By providing surface melt information at a higher spatial resolution of 500 m, UMelt allows for more precise and accurate detection of melt events. Additionally, UMelt captures short-lived melt events that may be missed by Sentinel-1 due to its low revisit time. This enhanced capability makes UMelt a valuable tool for studying and monitoring surface melt dynamics.

The UMelt record has the potential to provide valuable insights into specific melt dynamics that may be challenging to capture using Sentinel-1, ASCAT, or SSMIS. One notable application is the improved understanding of diurnal melt cycles, which provide valuable insights into the drivers and impacts of melt processes (Van Den Broeke et al., 2006). While ASCAT and SSMIS also provide temporal information, their coarse spatial resolution limits the ability to establish precise connections between surface melt patterns and local drivers. In contrast, UMelt enables us to examine highly localized melt triggers and track the evolving melt patterns throughout the day.

Another compelling research direction that utilizes the UMelt record involves monitoring surface melt on highly heterogeneous terrains, such as the Larsen C Ice Shelf. The Larsen C Ice Shelf is the largest remaining ice shelf on the Antarctic Peninsula and is vulnerable to potential collapse in a warming climate (Wang et al., 2022a). Notably, past disintegrations of Larsen A and Larsen B were preceded by elevated air temperatures and intense surface melt, underscoring the importance of understanding melt dynamics for assessing ice shelf stability (Banwell et al., 2013; Scambos et al., 2000, 2003). However, the spatial resolutions of ASCAT and SSMIS might be inadequate for accurately mapping surface melt along the grounding line of the Larsen C Ice Shelf. Depending solely on infrequent Sentinel-1 images that pass over the region a few times a week may restrict our comprehensive understanding of the intricate melt dynamics (see Fig. 1). Therefore, the UMelt record offers a promising addition to the currently existing remote sensing data for studying surface melt on highly heterogeneous ice shelves such as Larsen C.

4.2. Limitations of UMelt

Despite its promising capabilities, the UMelt product has inherent limitations due to the complex nature of its deep learning approach. The intricate workings of the model make it challenging to precisely identify the factors that contribute to the estimation of surface melt. While we have conducted assessments of the temporal performance (Fig. 5 and Supplementary Figure 2), spatial performance (Fig. 6), feature importance (Fig. 7), and transferability (Fig. 8) of the model, a complete understanding of its inner workings remains elusive. This is particularly evident in cases like Mary Byrd Land, where underestimation of surface melt is observed in melt season 2016–2017 (Fig. 9d). This highlights the need for further research and investigation to unravel the underlying mechanisms and improve the accuracy and performance of the UMelt product and/or the machine learning methods to develop such products.

Another limitation of deep learning networks is their tendency to mimic the patterns and characteristics they have been trained on. While UMelt incorporates inputs such as ASCAT and SSMIS, which provide real-time information about liquid water presence, it also considers elevation and multi-year Sentinel-1 melt fraction as input features. Given the current availability of Sentinel-1 data, the multi-year Sentinel-1 melt fraction input feature encompasses observations from both

Sentinel-1 A and -B, covering the period from 2016 (when Sentinel-1B was launched) to 2021 (when Sentinel-1B ceased operation). The model applies downscaling patterns based on past observations where ASCAT, SSMIS, elevation, and multi-year Sentinel-1 melt fraction collectively resulted in specific melt patterns. This means that when faced with unprecedented and dissimilar events that significantly deviate from its training data, the model may generate inaccurate results. This aligns with the insights presented in the study by Picard et al. (2007), which demonstrates that in regions with frequent melting, the number of melting days exhibits an almost continuous distribution, varying from year to year. Conversely, in areas where melting is infrequent, the distribution adopts an exponential pattern. In these cases, only a few years encounter a high number of melting days.

Finally, we utilized a basic Attention U-Net framework, which is renowned for its effectiveness in capturing spatial patterns in data (Oktay et al., 2018). A prospective advancement could involve integrating temporal information into the deep learning model, offering significant value for tasks that require the consideration of both spatial and temporal contexts to achieve accurate predictions. This holds true for surface melt prediction, as certain melt trends and patterns exhibit temporal dependencies throughout a melt season (Saunderson et al., 2022). A common approach for incorporating temporal information into U-Nets is through the utilization of 3D convolutional operations (Çiçek et al., 2016). While the 2D convolutions employed in our study operate on spatial dimensions (i.e., width and height), 3D convolutions additionally incorporate the temporal dimension (i.e., time or sequence). By leveraging these 3D convolutions, U-Nets can effectively capture spatiotemporal patterns, enabling the analysis and processing of data with combined spatial and temporal variations.

4.3. Implications of selected training region

The Shackleton Ice Shelf was selected as the training region, as it provided us with sufficient training data. While training a U-Net model on each individual ice shelf would be preferable, there are insufficient (or no) 'matching overpasses' available on most ice shelves to accomplish this (Fig. 2). Another advantage is that the Shackleton Ice Shelf exhibits a wide range of fine-scale melt patterns, especially along the grounding line and ice rises. The U-Net captured and represented these patterns well, and the results can be extrapolated to other ice shelves, as shown in Figs. 8 and 9.

One of the encountered limitations of selecting the Shackleton Ice Shelf as the training region is the presence of surface melt at relatively high elevations (up to 300 m), due to strong katabatic winds. This aligns with earlier research that identified that low-elevation regions near the grounding line in East Antarctica are frequently exposed to persistent katabatic winds (Arthur et al., 2020; Lenaerts et al., 2017; Stokes et al., 2019). As a consequence, UMelt could potentially overestimate surface melt in regions with less pronounced or absent katabatic winds. A study by Laffin et al. (2023) demonstrates that along the grounding line of the Shackleton Ice Shelf, roughly 50% of the melt is linked to downslope winds. Conversely, for the Larsen C Ice Shelf and the Abbot Ice Shelf, this proportion drops to less than 20%. A potential solution to address this issue is adjusting the current binary melt threshold, which is consistently set to 0.7, by implementing a region-specific threshold. Since the model is able to capture fine-scale melt patterns accurately, this approach may be effective.

4.4. Implications of selected reference data

UMelt was developed using Sentinel-1 as the reference data. We filled the observational gaps of Sentinel-1 and created a simulated Antarctic-wide product with a much higher temporal resolution (12 h) than the original Sentinel-1 data (1–7 days). However, while Sentinel-1 is a reliable source for melt detection, it has limitations.

First, Sentinel-1 fails to accurately detect the presence of liquid water in icy regions without snow cover (Zheng and Zhou, 2020; Zhou et al., 2019; de Roda Husman et al., 2022), such as on the southeast part of Shackleton or southeast part of Roi Baudouin ice shelves. Over these regions, Sentinel-1 is unable to differentiate between a dry and melting ice surface, as for both cases the backscatter intensity is very low (de Roda Husman et al., 2022). Consequently, in our UMelt product, we also encounter limitations in detecting melt over these regions, as demonstrated in Fig. 9b and 9e of our study. Using Sentinel-1 as the reference data has a further limitation regarding damaged ice. Damaged ice has heterogeneous surface orientations and thus different local incidence angles than the surrounding ice, leading to potential over- or underestimation of surface melt. We addressed this issue by excluding damaged areas from the U-Net development mask. A potential path for future improvement could be to use a different reference product for blue ice regions (e.g., using the blue ice maps of Hu et al., 2022; Jawak et al., 2023) and damaged areas (e.g., using the damage map of Izeboud and Lhermitte, 2023). Multispectral imagers, such as Landsat, MODIS, or Sentinel-2, may be suitable for this purpose. If such a merged, optimized reference product were available, the U-Net could be retrained to improve its performance.

Using Sentinel-1 as reference data presents another limitation, as it, like all microwave sensors, detects the presence of liquid water rather than directly observing the underlying energy conversion process of surface melt. It is important to highlight that both ASCAT and Sentinel-1 have a significant penetration depth, theoretically reaching up to 10 m (Ulaby et al., 1986). These large penetration depths enable them to potentially detect more residual water in the snowpack compared to SSMIS, which is limited to a theoretical penetration depth of 2.5 m (Ulaby et al., 1986). This could potentially explain the surface melt overestimation for ASCAT and Sentinel-1 (along with UMelt) compared to SSMIS over the Wilkins Ice Shelf, particularly at the end of the melt season (Fig. 9c). This is especially plausible given the known tendency of the Wilkins Ice Shelf to retain meltwater in the subsurface (Montgomery et al., 2020). A potential avenue for improving the UMelt record could involve assigning greater weight to SSMIS for locations with higher levels of retained melt. One possible approach to identifying these locations could involve examining the ASCAT and SSMIS time series and assessing the disparity between morning and afternoon observations. In areas with no active surface melt and only retained meltwater, it is more likely that the difference between morning and afternoon observations would be minimal towards the end of a melt season.

4.5. Downscaling other surface melt products

The findings of this study demonstrate the value of deep learning as a tool for monitoring surface melt with a high spatial and temporal resolution, offering insights into both historical and current ice shelf conditions. Additionally, other surface melt products, such as regional climate model data, can be utilized for downscaling surface melt.

Regional climate models typically operate at a resolution of tens of kilometers (e.g., Van Wessem et al., 2018; Agosta et al., 2019), which often fails to capture small-scale surface melt events occurring in Antarctica (Barrand et al., 2013). By incorporating deep learning models, it becomes possible to explore the relationship between large-scale melt patterns derived from regional climate models and fine-scale variations found in additional data sets, such as elevation data or multi-year Sentinel-1 melt fractions employed in this study. Hence, deep learning provides the capability to downscale coarse surface melt data derived from regional climate models.

The application of a U-Net proves to be a promising method for this purpose. By downscaling regional climate model data using deep learning techniques, we can gain a more comprehensive understanding of high-resolution surface melt. This not only encompasses the analysis of historical surface melt patterns but also enables the exploration of future projections.

5. Conclusion

This study presents a novel workflow to create a record of high-resolution surface melt on the Antarctic ice shelves, UMelt. The core of our approach is a modified U-Net that learns the patterns from high temporal (i.e., ASCAT and SSMIS) and high spatial (i.e., elevation and multi-year Sentinel-1 melt fraction) data. The trained model mimics the detailed Sentinel-1 melt observations but on a much higher temporal resolution, resulting in melt maps with a high spatial (500 m) and temporal (12 h) resolution.

We demonstrated the spatial and temporal transferability of the U-Net on the Shackleton Ice Shelf, achieving accuracies ranging from 87.2% to 95.5% for spatial transferability and 90.9% to 95.7% for temporal transferability. The U-Net also performed well in terms of spatiotemporal transferability, with good performance over the Larsen C Ice Shelf (91.0%). This spatiotemporal transferability allows for the assessment of surface melt on the entire Antarctic continent. The U-Net can provide maps of surface melt with a high resolution for all previous years with available input data, meaning we could study surface melt in high detail from 2006 (when ASCAT was launched) until present day. However, for both past and future scenarios, it is important to acknowledge that the model may necessitate re-training, especially when confronted with surface melt patterns that significantly differ from the training data used for the U-Net model.

High-resolution observations are crucial to monitor surface melt on the Antarctic ice shelves because of the short duration and fine melt patterns. Therefore, the high-resolution surface melt record on the Antarctic ice shelves UMelt provides a valuable product to be used in further studies, uncovering melt dynamics and potential consequent ice shelf instability that remains hidden in low-resolution satellite imagery.

Funding

S.R.H., S.L., S.S., and B.W. received support from the Nederlandse Organisatie voor Wetenschappelijk Onderzoek (NWO) under grant no. OCENW.GROOT.2019.091. M.I. was funded by the NWO and the Netherlands Space Office (NSO) under grant no. ALWGO.2018.043. Z.H. was funded by the NWO and NSO grant ALWGO.2018.039. D.L. was funded under NASA grant 80NSSC19K0057.

CRediT authorship contribution statement

Sophie de Roda Husman: Conceptualization, Methodology, Visualization, Writing – original draft, Data curation. **Stef Lhermitte:** Conceptualization, Supervision, Writing – review & editing, Methodology. **Jordi Bolibar:** Methodology, Writing – review & editing. **Maaike Izeboud:** Resources, Writing – review & editing. **Zhongyang Hu:** Methodology, Writing – review & editing. **Shashwat Shukla:** Methodology, Writing – review & editing. **Marijn van der Meer:** Methodology, Writing – review & editing. **David Long:** Resources, Writing – review & editing. **Bert Wouters:** Conceptualization, Methodology, Supervision, Writing – review & editing.

Declaration of competing interest

The authors declare that they have no known competing financial interests or personal relationships that could have appeared to influence the work reported in this paper.

Data availability

The scripts used to develop UMelt are available on GitHub at https://github.com/SdeRodaHusman/UMelt. The UMelt record, with a spatial resolution of 500 m and morning (6 AM) and afternoon (6 PM) observations for melt seasons 2016–2021, is accessible in two ways. First, as GeoTIFF files via 4TU.ResearchData (https://doi.org/10.4121/8a8934ef-9407-406f-8bfb-573eb182ec54.v1). Secondly, UMelt can be accessed as assets via Google Earth Engine. Users can access UMelt for specific melt seasons using the following link format: https://code.earthengine.google.com/?asset=projects/phd-detectionsurfacemelt/assets/UMelt_Antarctica/MeltSeasonXXXX/UMelt_AllData_MeltSeasonXXXX, where 'XXXX' should be replaced with the corresponding melt season. For example, replacing 'XXXX' with '1617' will provide the UMelt data for the 2016–2017 melt season. Similarly, replacing 'XXXX' with '1718', '1819', '1920', or '2021' will provide the UMelt data for the respective melt seasons. Users have the option to import UMelt into their Google Earth Engine environment using an example script provided on GitHub.

In addition to the UMelt record, melt occurrence data for a single melt season, as depicted in Fig. 9 and Supplementary Figure 2, are also available. These data can be downloaded from 4TU.ResearchData (https://doi.org/10.4121/8a8934ef-9407-406f-8bfb-573eb182ec54.v1) or accessed through Google Earth Engine (https://code.earthengine.google.com/?asset=projects/phd-detectionsurfacemelt/assets/UMelt_Antarctica/MeltSeasonXXXX/UMelt_MeltFraction_MeltSeasonXXXX).

Acknowledgments

The authors thank editor Menghua Wang, as well as Luke Trusel and an anonymous reviewer for their constructive comments.

During the preparation of this work, the authors used ChatGPT in order to enhance the readability of specific sections. After using this tool, the authors reviewed and edited the content as needed and take full responsibility for the content of the publication.

Appendix A. Supplementary data

Supplementary material related to this article can be found online at https://doi.org/10.1016/j.rse.2023.113950.

References

Agosta, C., Amory, C., Kittel, C., Orsi, A., Favier, V., Gallée, H., van den Broeke, M.R., Lenaerts, J., van Wessem, J.M., van de Berg, W.J., et al., 2019. Estimation of the Antarctic surface mass balance using the regional climate model MAR (1979–2015) and identification of dominant processes. Cryosphere 13 (1), 281–296.

Arthur, J.F., Stokes, C.R., Jamieson, S.S., Carr, J.R., Leeson, A.A., 2020. Distribution and seasonal evolution of supraglacial lakes on Shackleton Ice Shelf, East Antarctica. Cryosphere 14 (11), 4103–4120.

Ashcraft, I.S., Long, D.G., 2006. Comparison of methods for melt detection over Greenland using active and passive microwave measurements. Int. J. Remote Sens. 27 (12), 2469–2488.

Banwell, A.F., Datta, R.T., Dell, R.L., Moussavi, M., Brucker, L., Picard, G., Shuman, C.A., Stevens, L.A., 2021. The 32-year record-high surface melt in 2019/2020 on the northern George VI Ice Shelf, Antarctic Peninsula. Cryosphere 15 (2), 909–925.

Banwell, A.F., MacAyeal, D.R., Sergienko, O.V., 2013. Breakup of the Larsen B Ice Shelf triggered by chain reaction drainage of supraglacial lakes. Geophys. Res. Lett. 40 (22), 5872–5876.

Barrand, N.E., Vaughan, D.G., Steiner, N., Tedesco, M., Kuipers Munneke, P., Van Den Broeke, M.R., Hosking, J.S., 2013. Trends in Antarctic Peninsula surface melting conditions from observations and regional climate modeling. J. Geophys. Res.: Earth Surf. 118 (1), 315–330.

Baumhoer, C.A., Dietz, A.J., Kneisel, C., Kuenzer, C., 2019. Automated extraction of Antarctic glacier and ice shelf fronts from Sentinel-1 imagery using deep learning. Remote Sens. 11 (21), 2529.

Bengio, Y., 2012. Practical recommendations for gradient-based training of deep architectures. In: Neural Networks: Tricks of the Trade, second ed. Springer, pp. 437–478.

Bevan, S., Luckman, A., Hendon, H., Wang, G., 2020. The 2020 Larsen C Ice Shelf surface melt is a 40-year record high. Cryosphere 14 (10), 3551–3564.
Bevan, S.L., Luckman, A.J., Kuipers Munneke, P., Hubbard, B., Kulessa, B., Ashmore, D.W., 2018. Decline in surface melt duration on Larsen C Ice Shelf revealed by the advanced scatterometer (ASCAT). Earth Space Sci. 5 (10), 578–591.
Bolibar, J., Rabatel, A., Gouttevin, I., Galiez, C., Condom, T., Sauquet, E., 2020. Deep learning applied to glacier evolution modelling. Cryosphere 14 (2), 565–584.
Brodzik, M., Long, D., Hardman, M., Paget, A., Armstrong, R., 2016. MEaSUREs calibrated enhanced-resolution passive microwave daily EASE-grid 2.0 brightness temperature ESDR, version 1. NASA National Snow and Ice Data Center Distributed Active Archive Center.
Çiçek, Ö., Abdulkadir, A., Lienkamp, S.S., Brox, T., Ronneberger, O., 2016. 3D U-Net: learning dense volumetric segmentation from sparse annotation. In: Medical Image Computing and Computer-Assisted Intervention–MICCAI 2016: 19th International Conference, Athens, Greece, October 17-21, 2016, Proceedings, Part II 19. Springer, pp. 424–432.
Dahle, F., Tanke, J., Wouters, B., Lindenbergh, R., Dahle, F., Tanke, J., Wouters, B., Lindenbergh, R., 2022. Semantic segmentation of historical photographs of the Antarctica Peninsula. ISPRS Ann. Photogram. Remote Sens. Spatial Inf. Sci. 2, 237–244.
de Roda Husman, S., Hu, Z., Wouters, B., Munneke, P.K., Veldhuijsen, S., Lhermitte, S., 2022. Remote sensing of surface melt on Antarctica: Opportunities and challenges. IEEE J. Sel. Top. Appl. Earth Obs. Remote Sens..
Dirscherl, M., Dietz, A.J., Kneisel, C., Kuenzer, C., 2021. A novel method for automated supraglacial lake mapping in Antarctica using Sentinel-1 SAR imagery and deep learning. Remote Sens. 13 (2), 197.
Dupont, T., Alley, R., 2005. Assessment of the importance of ice-shelf buttressing to ice-sheet flow. Geophys. Res. Lett. 32 (4).
Gilbert, E., Kittel, C., 2021. Surface melt and runoff on Antarctic ice shelves at 1.5 C, 2 C, and 4 C of future warming. Geophys. Res. Lett. 48 (8), e2020GL091733.
Girshick, R., Donahue, J., Darrell, T., Malik, J., 2014. Rich feature hierarchies for accurate object detection and semantic segmentation. In: Proceedings of the IEEE Conference on Computer Vision and Pattern Recognition. pp. 580–587.
Gorelick, N., Hancher, M., Dixon, M., Ilyushchenko, S., Thau, D., Moore, R., 2017. Google Earth Engine: Planetary-scale geospatial analysis for everyone. Remote Sens. Environ. 202, 18–27.
Hofer, R., Mätzler, C., 1980. Investigations on snow parameters by radiometry in the 3-to 60-mm wavelength region. J. Geophys. Res.: Oceans 85 (C1), 453–460.
Howat, I.M., Porter, C., Smith, B.E., Noh, M.-J., Morin, P., 2019. The reference elevation model of Antarctica. Cryosphere 13 (2), 665–674.
Hu, Z., Munneke, P.K., Lhermitte, S., Dirscherl, M., Ji, C., van den Broeke, M., 2022. FABIAN: A daily product of Fractional Austral-summer Blue Ice over Antarctica during 2000–2021 based on MODIS imagery using Google Earth Engine. Remote Sens. Environ. 280, 113202.
Izeboud, M., Lhermitte, S., 2023. Damage detection on Antarctic ice shelves using the normalised radon transform. Remote Sens. Environ. 284, 113359.
Jawak, S.D., Luis, A.J., Pandit, P.H., Wankhede, S.F., Convey, P., Fretwell, P.T., 2023. Exploratory mapping of blue ice regions in Antarctica using very high-resolution satellite remote sensing data. Remote Sens. 15 (5), 1287.
Johnson, A., Fahnestock, M., Hock, R., 2020. Evaluation of passive microwave melt detection methods on Antarctic Peninsula ice shelves using time series of Sentinel-1 SAR. Remote Sens. Environ. 250, 112044.
Laffin, M.K., Zender, C.S., van Wessem, M., Noël, B., Wang, W., 2023. Wind-associated melt trends and contrasts between the greenland and Antarctic ice sheets. Geophys. Res. Lett. 50 (16), e2023GL102828.
Lenaerts, J., Lhermitte, S., Drews, R., Ligtenberg, S., Berger, S., Helm, V., Smeets, C., Van Den Broeke, M., Van De Berg, W.J., Van Meijgaard, E., et al., 2017. Meltwater produced by wind–Albedo interaction stored in an East Antarctic ice shelf. Nature Climate Change 7 (1), 58–62.
Lenaerts, J.T., Ligtenberg, S.R., Medley, B., Van de Berg, W.J., Konrad, H., Nicolas, J.P., Van Wessem, J.M., Trusel, L.D., Mulvaney, R., Tuckwell, R.J., et al., 2018. Climate and surface mass balance of coastal West Antarctica resolved by regional climate modelling. Ann. Glaciol. 59 (76pt1), 29–41.
Lhermitte, S., Sun, S., Shuman, C., Wouters, B., Pattyn, F., Wuite, J., Berthier, E., Nagler, T., 2020. Damage accelerates ice shelf instability and mass loss in Amundsen Sea Embayment. Proc. Natl. Acad. Sci. 117 (40), 24735–24741.
Liang, D., Guo, H., Zhang, L., Cheng, Y., Zhu, Q., Liu, X., 2021. Time-series snowmelt detection over the Antarctic using Sentinel-1 SAR images on Google Earth Engine. Remote Sens. Environ. 256, 112318.
Liu, H., Wang, L., Jezek, K.C., 2006. Spatiotemporal variations of snowmelt in Antarctica derived from satellite scanning multichannel microwave radiometer and Special Sensor Microwave Imager data (1978–2004). J. Geophys. Res.: Earth Surf. 111 (F1).
Massom, R.A., Scambos, T.A., Bennetts, L.G., Reid, P., Squire, V.A., Stammerjohn, S.E., 2018. Antarctic ice shelf disintegration triggered by sea ice loss and ocean swell. Nature 558 (7710), 383–389.
Mastrofini, M., Agostinelli, I., Curti, F., 2023. Design and validation of a U-Net-based algorithm for star sensor image segmentation. Appl. Sci. 13 (3), 1947.
Mohajerani, Y., Wood, M., Velicogna, I., Rignot, E., 2019. Detection of glacier calving margins with convolutional neural networks: A case study. Remote Sens. 11 (1), 74.
Montgomery, L., Miège, C., Miller, J., Scambos, T.A., Wallin, B., Miller, O., Solomon, D.K., Forster, R., Koenig, L., 2020. Hydrologic properties of a highly permeable firn aquifer in the Wilkins Ice Shelf, Antarctica. Geophys. Res. Lett. 47 (22), e2020GL089552.
Mote, T.L., Anderson, M.R., 1995. Variations in snowpack melt on the Greenland ice sheet based on passive-microwave measurements. J. Glaciol. 41 (137), 51–60.
Mousavi, M., Colliander, A., Miller, J.Z., Kimball, J.S., 2022. A novel approach to map the intensity of surface melting on the Antarctica ice sheet using SMAP L-band microwave radiometry. IEEE J. Sel. Top. Appl. Earth Obs. Remote Sens. 15, 1724–1743.
Nihashi, S., Ohshima, K.I., 2015. Circumpolar mapping of Antarctic coastal polynyas and landfast sea ice: Relationship and variability. J. Climate 28 (9), 3650–3670.
Niu, L., Tang, X., Yang, S., Zhang, Y., Zheng, L., Wang, L., 2023. Detection of Antarctic surface meltwater using sentinel-2 remote sensing images via U-net with attention blocks: A case study over the amery ice shelf. IEEE Trans. Geosci. Remote Sens..
Oktay, O., Schlemper, J., Folgoc, L.L., Lee, M., Heinrich, M., Misawa, K., Mori, K., McDonagh, S., Hammerla, N.Y., Kainz, B., et al., 2018. Attention U-Net: Learning where to look for the pancreas. arXiv preprint arXiv:1804.03999.
Olden, J.D., Jackson, D.A., 2002. Illuminating the "black box": A randomization approach for understanding variable contributions in artificial neural networks. Ecol. Model. 154 (1–2), 135–150.
Picard, G., 2022. Surface melt on the Antarctic and Greenland Ice Sheets (1979 - 2021). https://snow.univ-grenoble-alpes.fr/melting/. (Accessed 21 June 2023).
Picard, G., Fily, M., 2006. Surface melting observations in Antarctica by microwave radiometers: Correcting 26-year time series from changes in acquisition hours. Remote Sens. Environ. 104 (3), 325–336.
Picard, G., Fily, M., Gallée, H., 2007. Surface melting derived from microwave radiometers: A climatic indicator in Antarctica. Ann. Glaciol. 46, 29–34.
Picard, G., Leduc-Leballeur, M., Banwell, A.F., Brucker, L., Macelloni, G., 2022. The sensitivity of satellite microwave observations to liquid water in the Antarctic snowpack. Cryosphere Discussions 1–34.
Pritchard, H., Ligtenberg, S.R., Fricker, H.A., Vaughan, D.G., van den Broeke, M.R., Padman, L., 2012. Antarctic ice-sheet loss driven by basal melting of ice shelves. Nature 484 (7395), 502–505.
Radhakrishnan, K., Scott, K.A., Clausi, D.A., 2021. Sea ice concentration estimation: Using passive microwave and SAR data with a U-net and curriculum learning. IEEE J. Sel. Top. Appl. Earth Obs. Remote Sens. 14, 5339–5351.
Rignot, E., Mouginot, J., Scheuchl, B., Van Den Broeke, M., Van Wessem, M.J., Morlighem, M., 2019. Four decades of Antarctic Ice Sheet mass balance from 1979–2017. Proc. Natl. Acad. Sci. 116 (4), 1095–1103.
Roberts, D.R., Bahn, V., Ciuti, S., Boyce, M.S., Elith, J., Guillera-Arroita, G., Hauenstein, S., Lahoz-Monfort, J.J., Schröder, B., Thuiller, W., et al., 2017. Cross-validation strategies for data with temporal, spatial, hierarchical, or phylogenetic structure. Ecography 40 (8), 913–929.
Ronneberger, O., Fischer, P., Brox, T., 2015. U-net: Convolutional networks for biomedical image segmentation0. In: Medical Image Computing and Computer-Assisted Intervention–MICCAI 2015: 18th International Conference, Munich, Germany, October 5-9, 2015, Proceedings, Part III 18. Springer, pp. 234–241.
Saunderson, D., Mackintosh, A., McCormack, F., Jones, R.S., Picard, G., 2022. Surface melt on the Shackleton Ice Shelf, East Antarctica (2003–2021). Cryosphere 16 (10), 4553–4569.
Scambos, T., Hulbe, C., Fahnestock, M., 2003. Climate-induced ice shelf disintegration in the Antarctic Peninsula. In: Antarctic Peninsula Climate Variability: Historical and Paleoenvironmental Perspectives, Vol. 79. Wiley Online Library, pp. 79–92.
Scambos, T.A., Hulbe, C., Fahnestock, M., Bohlander, J., 2000. The link between climate warming and break-up of ice shelves in the Antarctic Peninsula. J. Glaciol. 46 (154), 516–530.
Stokes, C.R., Sanderson, J.E., Miles, B.W., Jamieson, S.S., Leeson, A.A., 2019. Widespread distribution of supraglacial lakes around the margin of the East Antarctic Ice Sheet. Sci. Rep. 9 (1), 13823.
Torinesi, O., Fily, M., Genthon, C., 2003. Variability and trends of the summer melt period of Antarctic ice margins since 1980 from microwave sensors. J. Clim. 16 (7), 1047–1060.
Trebing, K., Stańczyk, T., Mehrkanoon, S., 2021. SmaAt-UNet: Precipitation nowcasting using a small attention-UNet architecture. Pattern Recognit. Lett. 145, 178–186.
Trusel, L., Frey, K.E., Das, S.B., 2012. Antarctic surface melting dynamics: Enhanced perspectives from radar scatterometer data. J. Geophys. Res.: Earth Surf. 117 (F2).
Trusel, L.D., Frey, K.E., Das, S.B., Karnauskas, K.B., Munneke, P.K., Van Meijgaard, E., Van Den Broeke, M.R., 2015. Divergent trajectories of Antarctic surface melt under two twenty-first-century climate scenarios. Nat. Geosci. 8 (12), 927–932.
Trusel, L.D., Frey, K.E., Das, S.B., Munneke, P.K., Van Den Broeke, M.R., 2013. Satellite-based estimates of Antarctic surface meltwater fluxes. Geophys. Res. Lett. 40 (23), 6148–6153.
Ulaby, F.T., Long, D., 2014. Microwave Radar and Radiometric Remote Sensing. University of Michigan Press.
Ulaby, F.T., Moore, R.K., Fung, A.K., 1986. Microwave remote sensing: Active and passive. Volume 3-From theory to applications.
van den Broeke, M., 2005. Strong surface melting preceded collapse of Antarctic Peninsula ice shelf. Geophys. Res. Lett. 32 (12).

Van Den Broeke, M., Reijmer, C., Van As, D., Boot, W., 2006. Daily cycle of the surface energy balance in Antarctica and the influence of clouds. Int. J. Climatol.: J. R. Meteorol. Soc. 26 (12), 1587–1605.

van der Meer, M., de Roda Husman, S., Lhermitte, S., 2023. Deep learning regional climate model emulators: A comparison of two downscaling training frameworks. J. Adv. Modelling Earth Syst. 15 (6), e2022MS003593.

van Wessem, J.M., van den Broeke, M.R., Wouters, B., Lhermitte, S., 2023. Variable temperature thresholds of melt pond formation on Antarctic ice shelves. Nature Clim. Change 13 (2), 161–166.

Van Wessem, J.M., Van De Berg, W.J., Noël, B.P., Van Meijgaard, E., Amory, C., Birnbaum, G., Jakobs, C.L., Krüger, K., Lenaerts, J., Lhermitte, S., et al., 2018. Modelling the climate and surface mass balance of polar ice sheets using RACMO2–Part 2: Antarctica (1979–2016). Cryosphere 12 (4), 1479–1498.

Wang, S., Liu, H., Jezek, K., Alley, R.B., Wang, L., Alexander, P., Huang, Y., 2022a. Controls on Larsen C ice shelf retreat from a 60-year satellite data record. J. Geophys. Res.: Earth Surf. 127 (3), e2021JF006346.

Wang, X., Qiu, Y., Zhang, Y., Lemmetyinen, J., Cheng, B., Liang, W., Leppäranta, M., 2022b. A lake ice phenology dataset for the Northern Hemisphere based on passive microwave remote sensing. Big Earth Data 1–19.

Wei, Y., Li, X., Gu, L., Zheng, X., Jiang, T., Zheng, Z., 2022. A fine-resolution snow depth retrieval algorithm from enhanced-resolution passive microwave brightness temperature using machine learning in Northeast China. IEEE Geosci. Remote Sens. Lett. 19, 1–5.

Wille, J.D., Favier, V., Dufour, A., Gorodetskaya, I.V., Turner, J., Agosta, C., Codron, F., 2019. West Antarctic surface melt triggered by atmospheric rivers. Nat. Geosci. 12 (11), 911–916.

Wilmes, S.-B., Green, J.M., Gomez, N., Rippeth, T.P., Lau, H., 2017. Global tidal impacts of large-scale ice sheet collapses. J. Geophys. Res.: Oceans 122 (11), 8354–8370.

Zhang, Q., Wu, Y.N., Zhu, S.-C., 2018. Interpretable convolutional neural networks. In: Proceedings of the IEEE Conference on Computer Vision and Pattern Recognition. pp. 8827–8836.

Zhao, J., Liang, S., Li, X., Duan, Y., Liang, L., 2022. Detection of surface crevasses over Antarctic ice shelves using SAR imagery and deep learning method. Remote Sens. 14 (3), 487.

Zheng, L., Zhou, C., 2020. Comparisons of snowmelt detected by microwave sensors on the Shackleton Ice Shelf, East Antarctica. Int. J. Remote Sens. 41 (4), 1338–1348.

Zhou, C., Zheng, L., Sun, Q., Liu, R., 2019. Amery Ice Shelf surface snowmelt detected by ASCAT and Sentinel-1. Remote Sens. Lett. 10 (5), 430–438.

Zwally, H.J., Fiegles, S., 1994. Extent and duration of Antarctic surface melting. J. Glaciol. 40 (136), 463–475.